

Synthesis of an Ni₂P catalyst supported on Na-MCM-41 with highly activity for dibenzothiophene HDS under mild conditions

Hua Song¹  · Fuyong Zhang¹ · Nan Jiang¹ · Maosen Chen¹ · Feng Li¹ · Zijin Yan¹

Received: 9 October 2017 / Accepted: 2 April 2018
© Springer Science+Business Media B.V., part of Springer Nature 2018

Abstract A novel and simple method to synthesize supported Ni₂P/Na(*x*)-MCM-41 catalysts (where *x* is the mass fraction of Na-to-MCM-41 in terms of percentage) at a lower reduction temperature by incorporation of Na was described. The catalysts were characterized by H₂ temperature-programmed reduction (H₂-TPR), X-ray diffraction (XRD), N₂ adsorption-desorption, CO uptake, X-ray photoelectron spectroscopy (XPS), and transmission electron microscopy (TEM). The effect of Na on the structure of catalysts and catalytic properties for the dibenzothiophene (DBT) hydrodesulfurization (HDS) was investigated, which confirmed that a suitable amount of Na can promote highly dispersed Ni₂P particles. The Na preferentially interacts with phosphate to generate the sodium phosphate and therefore suppresses the formation of stronger P–O–P bonds, which enables the phosphide catalyst to be easily formed at a lower reduction temperature. Compared with conventional phosphate (973–1273 K), the reduction temperature of Ni₂P/Na(*x*)-MCM-41 catalyst was relatively low (773 K). The Ni₂P/Na(*x*)-MCM-41 catalyst with *x* = 1.0 showed the maximum DBT conversion of 91.6%, which is higher than that of Ni₂P/M41 without Na (80.3%).

Keywords Ni₂P · Na-MCM-41 · Sodium · Hydrodesulfurization · Dibenzothiophene

Electronic supplementary material The online version of this article (<https://doi.org/10.1007/s11164-018-3423-z>) contains supplementary material, which is available to authorized users.

✉ Hua Song
songhua2004@sina.com

¹ Provincial Key Laboratory of Oil and Gas Chemical Technology, College of Chemistry and Chemical Engineering, Northeast Petroleum University, Daqing 163318, Heilongjiang, China

Introduction

It is well known that the current commercial hydrodesulfurization (HDS) catalysts, such as sulfides catalysts [1], are not up to the regulated levels [2]. Therefore, development of new types of deep HDS catalysts has drawn great attention. Transition metal phosphides have recently received extensive attention as a new family of non-sulfided HDS catalysts because they exhibit higher HDS activity [3, 4]. Among these, Ni_2P showed the highest HDS activity [5, 6].

Some previous studies [7, 8] have shown that Ni_2P catalysts were prepared by H_2 temperature-programmed reduction (TPR) of oxidic precursors. The TPR method is convenient and simple; however, it requires high reduction temperature for the phosphate species mainly because the strong P–O bond in phosphate, which requires much energy and a long production time. Therefore, it is necessary to explore novel approaches featuring mild conditions for preparation of Ni_2P catalyst. Recently, there have been reports of some new approaches for preparing Ni_2P catalysts. Berhault et al. [9] found that unsupported nickel phosphides could be produced by nickel thiophosphate (NiPS_3) at lower temperatures. Lee [10] reported a liquid-phase phosphidation method by which Ni_2P nanostructures can be obtained by co-reaction of nickel acetylacetonate ($\text{Ni}(\text{acac})_2$) with trioctylphosphine (TOP) in coordinating solvent trioctylphosphine oxide (TOPO) at 573 K. Our previous study [11, 12] used $\text{Ni}(\text{acac})_2$ and low-cost triphenylphosphine (TPP) in the presence of the coordinating solvent tri-*n*-octylamine (TOA) to synthesize Ni_2P catalyst at 603 K in an N_2 atmosphere. It is well known that the reduction temperature could be effectively decreased by using low-state phosphide instead of high-state phosphide. Our group also found Ni_2P catalysts can be successfully prepared by H_2 reduction of a mixture of $\text{NH}_4\text{H}_2\text{PO}_2$ and $\text{NiCl}_2 \cdot 6\text{H}_2\text{O}$ precursor at low temperature, and with this preparation method, the catalysts do not need to be calcined, which saved energy [13]. Brussell et al. [14] reported a novel preparation method of Ni_2P catalysts, in which the hypophosphite-based precursor (H_3PO_2) was used instead of high-state phosphide phosphorus salts. One of its advantages is that it can be conducted under mild conditions. But so far, most of the methods reported used different phosphide precursors such as low-state phosphide to reduce the reduction temperature of the Ni_2P catalysts. Sawada [15] found that the reduction temperatures of Rh_2P supported on Al_2O_3 and SiO_2 catalysts could be reduced by adding metal sodium (Na) to the corresponding catalyst, showing that metal Na plays an important role in reducing the reduction temperature of catalysts. Therefore it appears reasonable to speculate that metal Na could affect the reduction temperature of Ni_2P catalyst precursor and promote the HDS activity of Ni_2P catalyst. However, to the best of our knowledge, up to now, there are no reported works focused on the influence of Na on the reduction of Ni_2P catalysts under mild conditions and the performance of HDS. Therefore, it is interesting to study the effect of Na on the reduction of Ni_2P precursor under mild conditions and HDS performance of Ni_2P catalyst for refractory sulfur compounds such as dibenzothio-*phene* (DBT).

In this paper, Ni₂P/Na-MCM-41 catalysts were successfully prepared by the TPR method with Na-doped Na-MCM-41 support at a low reduction temperature of 773 K. The effect of Na mass fraction on the structure of catalysts and catalytic properties for DBT HDS were studied.

Experimental

Preparation of supports and catalysts

Siliceous MCM-41 was synthesized using tetraethyl orthosilicate (TEOS) as the silica source and cetyltrimethylammonium bromide (CTAB) as the template, following the procedure as described in the literature [16]. The Na-doped MCM-41 support was prepared by impregnation of the NaNO₃ aqueous solution with MCM-41 support, and then the water was evaporated to obtain a solid product. The impregnated supports were dried at 383 K for 24 h and calcined at 673 K for 1 h (with a heating rate of 2.5 K min⁻¹). The supports obtained were named 'M41' for MCM-41 and 'Na(*x*)M41' for Na-MCM-41, where *x* is the mass fraction of Na-to-M41 in terms of percentage.

The supported Ni₂P catalyst precursors were prepared by impregnating diammonium hydrogen phosphate ((NH₄)₂HPO₄) and nickel nitrate hexahydrate (Ni(NO₃)₂·6H₂O) solution with the mesoporous supports. The precursors were prepared with Ni loading of 9.73 wt%, and the initial Ni-to-P molar ratios was 1:2. In a typical synthesis technique, (NH₄)₂HPO₄ and Ni(NO₃)₂·6H₂O were dissolved in deionized water at room temperature to form a uniform solution. The M41 and Na(*x*)M41 were wet-impregnated with the above solution for 12 h. After the water was evaporated, the resulting solid was dried at 393 K for 12 h and calcined at 773 K for 3 h to obtain the final oxidic precursor.

The catalyst precursors were reduced in a fixed-bed reactor by heating from room temperature to 773 K at a rate of 2.0 K min⁻¹ in a flow of H₂ (200 mL min⁻¹) and held for 2 h. The obtained catalysts were allowed to cool naturally to room temperature in a continuous H₂ flow and then passivated in an O₂/N₂ mixture (0.5 vol.% O₂) with a flow rate of 20 mL min⁻¹ for 2 h. The corresponding catalysts are denoted as Ni₂P/M41 and Ni₂P/Na(*x*)M41, respectively.

Characterization of catalysts

The reducibility of precursors was characterized by the H₂ TPR (H₂-TPR) using a PC-1200 gas adsorption analyzer, in which 0.05 g of the precursors was loaded in a quartz U tube reactor, and reduced in flow of a 10 vol.% H₂/Ar (20 mL min⁻¹) at a heating rate of 5 K min⁻¹. The TPR spectrum was determined using a thermal conductivity detector (TCD) to monitor hydrogen consumption.

The small-angle XRD patterns were obtained with a RINT2000-X-ray diffractometer using Cu K α radiation under the setting conditions of 35 kV, 50 mA, scan range from 0.5° to 10° at a rate of 1/6 °C min⁻¹. The large-angle XRD analysis was carried out on a D/max-2200PC-X-ray diffractometer using Cu K α radiation under

the setting conditions of 40 kV, 30 mA, scan range from 10 to 80° at a rate of 10° min⁻¹.

N₂ adsorption–desorption was carried out on a NOVA2000e instrument at 77 K. All the sample was pretreated at 473 K for 2 h until the vacuum pressure was 6 mm Hg before measurement.

CO uptake measurements were performed by using a Setaram Tian-Calvet C-80 heat-flux microcalorimeter. Passivated catalyst (0.1 g) was loaded in the reactor and reduced in a H₂ flow (30 mL min⁻¹) at 500 °C for 1 h. After pretreatment in a continuous He flow and cooling the sample to room temperature, CO pulses were injected into He, and the CO uptake was measured using a TCD until there was no further CO adsorption after consecutive injections.

Transmission electron microscopy (TEM) examinations were performed using a JEOL JEM-2100 instrument operated at 200 kV. The powder samples were ultrasonically dispersed in ethanol and placed on a carbon-coated copper grid.

The XPS spectra were acquired using an ESCALAB MKII spectrometer, using monochromatic Mg K α radiation ($E = 1253.6$ eV) and equipped with a hemispherical analyzer operating at fixed pass energy of 40 eV. The recorded photoelectron binding energies were referenced against the C 1s contamination line at 284.8 eV.

Catalytic activities

The HDS of DBT over prepared catalysts was performed in a flowing high-pressure fixed-bed reactor using a feed consisting of a decalin solution of DBT (1 wt%). The conditions of the HDS reaction were 613 K, 3.0 MPa, WHSV = 2.5 h⁻¹, and hydrogen-to-oil ratio of 550 (V/V). Prior to reaction, 0.8 g of the catalysts were pretreated in situ with flowing H₂ (30 mL min⁻¹) at 773 K for 2 h. The liquid products of HDS reaction was collected and analyzed by flame ionization detector (FID) gas chromatography (GC) with a GC-14C-60 column. Turnover frequency (TOF) values of the samples containing nickel phosphide were calculated using Eq. (1) [17]:

$$\text{TOF} = \frac{F X}{W M} \quad (1)$$

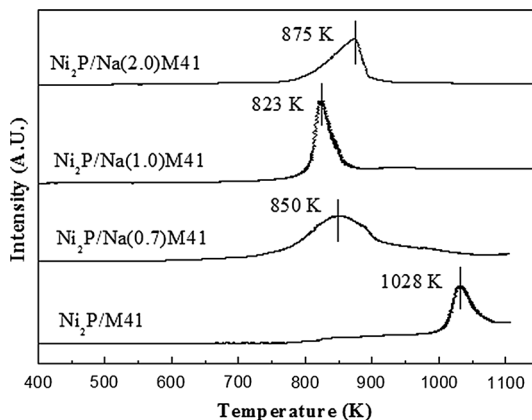
where F is the molar rate of DBT fed into the reactor (mol s⁻¹), X is the conversion of DBT (%), W is the weight of catalyst (g), and M is the mole of sites loaded which is decided by the CO uptake.

Results and discussion

H₂-TPR

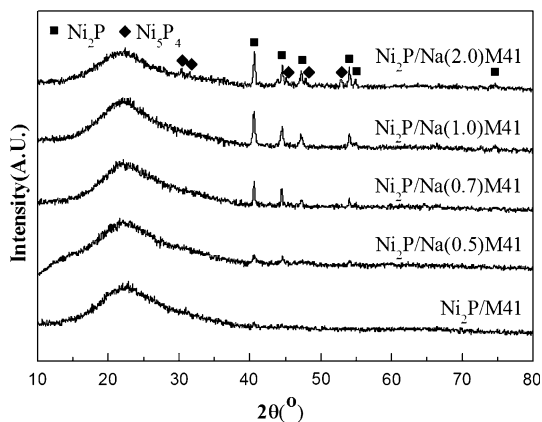
The H₂-TPR profiles of the Ni₂P/M41 and Ni₂P/Na(x)M41 catalyst precursors are shown in Fig. 1. It can be observed that the reduction of Ni₂P/M41 precursors started around 910 K and the reduction peak was centered at 1028 K, which can be

Fig. 1 H₂-TPR profiles of the Ni₂P/M41 and Ni₂P/Na(x)M41 catalyst precursors



ascribed to the reduction of highly thermodynamically stable P–O–P bonds and the co-reductions of the nickel species in phosphate [18]. The reduction of Ni₂P/Na(x)M41 precursors started around 760 K and the reduction peaks were shifted to a much lower region, indicating that the incorporation of Na into the Ni₂P/M41 could significantly decrease the reduction temperature. This is possibly because the Na preferentially interacts with phosphate to generate the sodium phosphate and therefore suppresses formation of stronger P–O–P bonds, which can produce the phosphide catalyst at a lower reduction temperature [15]. A more detailed discussion is shown in Sect. 3.8. With increasing the Na mass fraction, the reduction temperature decreased to 823 K and then increased to 875 K, showing that addition of too much Na increases the reduction temperature. This is possibly because the excess Na causes formation of small amounts of the Ni₅P₄ phase (Fig. 2, XRD analysis), which suppresses formation of Ni₂P to some extent.

Fig. 2 XRD patterns of the Ni₂P/Na(x)M41 catalysts



XRD

Figure S1 illustrates the small-angle XRD patterns of the M41 and Na(1.0)M41 supports. The M41 indicated some peaks at $2\theta = 1.2\text{--}6^\circ$ corresponding to 100, 110, 200, and 210 planes of the typical long hexagonal structure of M41. The Na(1.0)M41 exhibited similar peaks. However, the peaks were slightly shifted to higher angle values and intensities became lower, which indicates that a certain amount of Na atoms could cause some deformation or distortion of the original M41 tetrahedral coordination structure. Figure S2 shows the small-angle XRD patterns of the Ni₂P/M41 and Ni₂P/Na(1.0)M41 catalysts. Upon loading Ni₂P, the diffraction peaks were shifted to higher angle values and the intensities became lower as compared to original supports, showing that loading Ni₂P causes some lattice distortion or lattice collapse.

The XRD patterns of Ni₂P/Na(x)M41 catalysts with different Na mass fractions are shown in Fig. 2. As can be seen from Fig. 2, all samples exhibit a broad feature owing to the amorphous nature of mesoporous Na(x)M41 at $2\theta \approx 22^\circ$. Furthermore, the Ni₂P/Na(x)M41 samples also showed peaks of Ni₂P at $2\theta = 40.6, 44.5, 47.1$ and 54.1° (PDF: 03-0953). This indicates that Ni₂P is the main active phase for all samples. The Ni₂P/M41 showed relatively weak peaks of Ni₂P, while the peaks of Ni₂P phase for the Ni₂P/Na(x)M41 samples become more intense. In addition, with increasing the Na mass fraction, the peaks intensities increased, which reveals the Na can promote formation of Ni₂P. This showed that incorporation of Na could promote formation of more and higher-crystallinity Ni₂P phase. Moreover, the Ni₂P/Na(2.0)M41 exhibits some weak diffraction peaks at $30.3, 31.5, 45.1, 49.7^\circ$ and 52.9° (PDF: 18-0883) owing to small amounts of the Ni₅P₄ phase, which indicates that excess Na suppresses the reduction of PO₃⁴⁻ into Ni₂P. The D_c of the Ni₂P crystallites estimated by Scherrer's equation [19, 20] is listed in column 5 of Table 1. The crystallite size (D_c) of Ni₂P/Na(0.5)M41 was 22.5 nm. With increasing the Na mass fraction, the Ni₂P particles increased, which shows that the crystallinity of Ni₂P phase increased. In other words, this result also shows that the incorporation of Na can decrease the reduction temperature of Ni₂P. Sawada [20] similarly showed addition of Na can decrease the reduction temperature of Rh₂P and promote the formation of the active Rh₂P phase.

N₂ adsorption–desorption

Table 1 illustrates the textural properties of Na(x)M41 support and Ni₂P/Na(x)M41 samples. The surface area and pore volume of the M41 support were $910.6 \text{ m}^2 \text{ g}^{-1}$ and $0.96 \text{ cm}^3 \text{ g}^{-1}$, respectively. Upon incorporating Na into M41, a decrease in specific surface area (S_{BET}) of Na(x)M41 was observed, accompanied with decreases in pore volume (V_p) and pore diameter (d). In addition, with increase of Na mass fraction, the S_{BET} , V_p and d became much smaller, showing that the Na was incorporated into the pores of the sieves. In parallel, a remarkable drop in the S_{BET} and V_p of the Ni₂P/Na(x)M41 catalysts was observed after loading Ni₂P, when compared with the corresponding supports. This indicates that the pores of supports were blocked by Ni₂P. Moreover, the surface area of Ni₂P/Na(x)M41 indicated a

Table 1 The properties and HDS catalytic performance of the catalysts

Sample	S_{BET} (m ² g ⁻¹)	V_p (cm ³ g ⁻¹)	d (nm)	D_c (nm) ^a	CO uptake (μmol g ⁻¹)	Conversion (%) 553 K	Selectivity (%)		TOF (10 ⁻³ s ⁻¹)
							CHB	BP	
M41	910.6	0.962	4.23	-	-	-	-	-	-
Na(0.5)M41	871.3	0.891	4.12	-	-	-	-	-	-
Na(0.7)M41	857.6	0.874	4.08	-	-	-	-	-	-
Na(1.0)M41	753.9	0.709	3.76	-	-	-	-	-	-
Na(2.0)M41	639.8	0.591	3.69	-	-	-	-	-	-
Ni ₂ P/M41	268.2	0.227	3.21	-	28	40.62	14.8	85.2	3.2
Ni ₂ P/Na(0.5)M4	291.7	0.312	4.28	22.5	33	49.50	14.9	85.1	3.3
Ni ₂ P/Na(0.7)M41	286.5	0.309	4.41	25.7	40	59.05	15.2	84.8	3.4
Ni ₂ P/Na(1.0)M41	165.6	0.189	4.61	26.1	51	62.35	16.9	83.1	3.6
Ni ₂ P/Na(2.0)M41	74.8	0.126	7.11	32.0	47	55.83	15.1	84.9	3.4

^aCalculated from $D_c = K\lambda/\beta \cos(\theta)$, the Scherrer equation, based on the Ni₂P {1 1 1}

dramatic decreased upon increasing the Na mass fraction. The S_{BET} of $\text{Ni}_2\text{P}/\text{Na}(1.0)\text{M41}$ was almost two-fold when compared with that found for $\text{Ni}_2\text{P}/\text{Na}(2.0)\text{M41}$, showing the growth of the Ni_2P particle sizes (Table 1, D_c obtained by XRD), which resulted in the decrease of S_{BET} .

The N_2 adsorption–desorption isotherms of the supports and catalysts are presented in Fig. 3. As can be seen from Fig. 3, all the supports and catalysts exhibited a type IV isotherm and a standard H4 type hysteresis loop according to the IUPAC classification, which reveals that some mesopores are present for all samples.

CO uptake

The CO adsorption was used to estimate the surface density of exposed Ni sites on the catalysts [21]. The CO uptakes at room temperature of the $\text{Ni}_2\text{P}/\text{M41}$ and $\text{Ni}_2\text{P}/\text{Na}(x)\text{M41}$ catalysts are listed in column 6 of Table 1. Actually, CO molecules may also be adsorbed on the surface of P sites. However, because of the relatively small amount, it can be ignored in the following discussion [22]. As shown in Table 1, the CO uptake of the $\text{Ni}_2\text{P}/\text{M41}$ catalyst was $28 \mu\text{mol g}^{-1}$. Upon incorporation of Na, the CO uptakes of the $\text{Ni}_2\text{P}/\text{Na}(x)\text{M41}$ catalysts were increased. In addition, with increasing the Na mass fraction, the CO uptakes of the $\text{Ni}_2\text{P}/\text{Na}(x)\text{M41}$ catalysts increased initially and decreased after a maximal value was achieved. These results showed that an appropriate amount of Na can promote more exposed nickel atoms on the surface. The amount of exposed Ni atoms over the catalyst is mainly affected by two factors, on one hand, by the amount of the active Ni_2P particles and their dispersion, and on the other hand, by the P and Na coverage on the surface of catalyst. With increasing the Na mass fraction (< 1.0), more Ni_2P particles were formed (XRD analysis) and a better dispersion of the active Ni_2P phase (TEM analysis, will discuss later) can be achieved. Compared with Na, the P was presented in a relatively large proportion. Therefore, at lower Na content (< 1.0), the P coverage is the key factor. With addition and increasing the Na mass fraction (< 1.0), the surface P-to-Ni ratio decreased significantly. For all these reason, the CO uptake increased with increasing the Na mass fraction. However, when Na mass

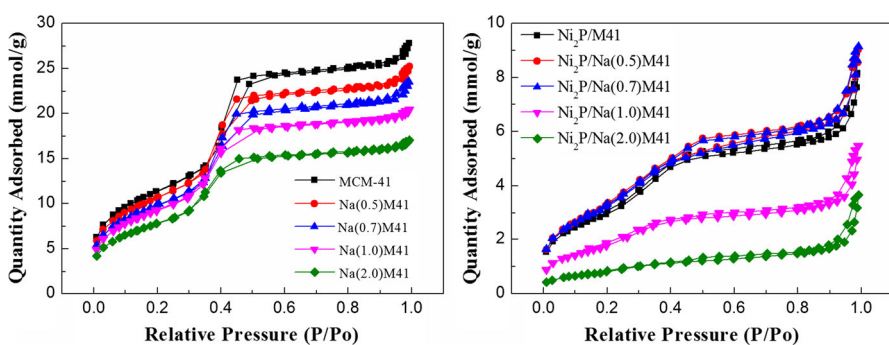


Fig. 3 The nitrogen adsorption/desorption isotherms for M41, $\text{Na}(x)\text{M41}$, and $\text{Ni}_2\text{P}/\text{Na}(x)\text{M41}$ catalysts

fraction increased from 1.0 to a relatively higher value of 2.0, the surface P-to-Ni ratio increased instead of decreased (Table 2, XPS analysis). Therefore, the coverage of P and Na became more impactful, occupying some of the Ni sites and leading to a lower CO uptake of Ni₂P/Na(2.0)M41. In addition, the growth in Ni₂P particle sizes and decrease in surface area (See Table 1), which lead to poor dispersion, were other reasons for the lower CO uptake of Ni₂P/Na(2.0)M41.

XPS

XPS patterns were used to further identify the influence of Na mass fraction on the catalysts and its surface composition. Figure 4 illustrates the XPS spectra of the Ni₂P/M41 and Ni₂P/Na(x)M41 samples in the Ni(2*p*) and P(2*p*) regions, and Table 2 shows the binding energies and the P-to-Ni atomic ratios for all samples. As shown in Fig. 4, all spectra were decomposed, taking into account the spin-orbital splitting of the Ni 2*p*_{3/2} and Ni 2*p*_{1/2} lines (about 17 eV) and the presence of satellite peaks at about 5 eV higher than the binding energy of the parent signal [23]. It is well known that Ni 2*p*_{3/2} core-level spectrum consists of three components. The bands centered at 852.4–852.6 eV can be ascribed to Ni^{δ+} in the Ni₂P phase. The second at 856.5–856.9 eV corresponds to the Ni²⁺ species interacting with phosphate species as a consequence of superficial passivation. This is accompanied with the broad satellite at approximately 5.0 eV higher than that of the Ni²⁺ species and this shake-up peak is assigned to divalent species [24]. Other broad peaks on the high-binding-energy side can be assigned to the Ni 2*p*_{1/2} signal from oxidized Ni species [25]. P 2*p* binding energy involves the peaks at 128.9–129.3 eV can be assigned to P^{δ-} species on the metal phosphides [23] and the peak at 134.6–134.8 eV is due to phosphate (P⁵⁺) arising from superficial oxidation of nickel phosphide particles [26].

As can be seen from Fig. 4a and Table 2, the XPS spectra for the as-prepared Ni₂P/M41 exhibited Ni 2*p* peaks at 852.6 and 856.9 eV, which can be attributed to the Ni^{δ+} band forming a Ni₂P phase and Ni²⁺ species, respectively. No obvious change can be seen for the binding energy of Ni species between the Ni₂P/Na(x)M41 and Ni₂P/M41. However, the peaks of Ni^{δ+} and Ni²⁺ species shift to a

Table 2 Spectral parameters obtained by XPS analysis for the catalysts

Sample	Binding energy (eV)					Superficial atomic ratio		
	Ni 2 <i>p</i> _{3/2}			P 2 <i>p</i> _{3/2}		Na-to-Ni	P-to-Ni	Na-to-P
	Ni ^{δ+}	Satellite	Ni ^{δ+}	P ⁵⁺	P ^{δ-}			
Ni ₂ P/M41	856.9	861.7	852.6	134.8	128.9	–	3.14	–
Ni ₂ P/Na(0.5)M41	856.7	861.5	852.5	134.6	129.3	0.20	2.12	0.09
Ni ₂ P/Na(0.7)M41	856.6	861.7	852.4	134.8	129.3	0.21	1.96	0.11
Ni ₂ P/Na(1.0)M41	856.5	861.8	852.4	134.6	129.3	0.23	1.84	0.13
Ni ₂ P/Na(2.0)M41	856.8	862.2	852.6	134.8	129.2	0.40	1.95	0.21

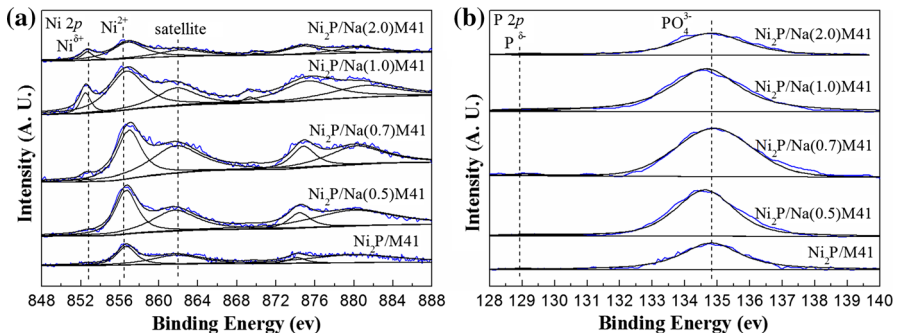


Fig. 4 XPS spectra of the $\text{Ni}_2\text{P}/\text{Na}(x)\text{M41}$ catalysts

slightly lower value with the incorporation of Na. This result shows that there is interaction between the Ni_2P particles and $\text{Na}(x)\text{M41}$ support. In addition, it is worth noting that the intensity of the $\text{Ni}^{\delta+}$ species peaks located around 852.4 eV initially increased, reaching a maximum value at $x = 1.0$, and then decreased with further increasing Na mass fraction in the catalyst. This indicates more Ni_2P particles may be exposed on the surface of $\text{Ni}_2\text{P}/\text{Na}(x)\text{M41}$ and the incorporation of Na can promote the formation of Ni_2P phase. This result were also confirmed by XRD. As can be seen from Fig. 4b, for $\text{Ni}_2\text{P}/\text{M41}$, the peaks centered at 134.8 eV for PO_4^{3-} was observed, together with a low intensity peak at 128.9 eV that can be attributed to the $\text{P}^{\delta-}$ band forming Ni_2P . However, the binding energies of $\text{P}^{\delta-}$ over the $\text{Ni}_2\text{P}/\text{Na}(x)\text{M41}$ catalysts are slightly higher than the value reported for $\text{Ni}_2\text{P}/\text{M41}$ (128.9 eV) without Na addition. This shows the incorporation of Na can lead to a small charge transfer from Ni to P in the catalyst [27]. This special effect favors the reduction of PO_3^{4-} into Ni_2P . Therefore, an appropriate amount of Na ($x = 1.0$) incorporated can promote the formation of active Ni_2P phase.

Table 2 summarizes the binding energy and the surface Na-to-Ni, P-to-Ni, and Na-to-P atomic ratios for the $\text{Ni}_2\text{P}/\text{M41}$ and $\text{Ni}_2\text{P}/\text{Na}(x)\text{M41}$ catalysts. The initial P-to-Ni ratio corresponding to the precursor materials was 2:1. However, the surface P-to-Ni ratio of $\text{Ni}_2\text{P}/\text{M41}$ was 3.14, which is higher than the initial P-to-Ni ratio. This is due to the enrichment of phosphorous on the surface of the catalysts. Note that upon addition of Na, the surface P-to-Ni ratio of $\text{Ni}_2\text{P}/\text{M41}$ decreased remarkably. With addition and increasing the Na mass fraction (< 1.0), the P-to-Ni ratio decreased. This shows that the incorporation of Na could suppress the enrichment of P on the surface, which could lead to the increase in the exposed nickel sites on the surface. The CO uptake analysis confirmed this. The $\text{Ni}_2\text{P}/\text{Na}(2.0)\text{M41}$ showed a slightly higher P-to-Ni ratio than that of $\text{Ni}_2\text{P}/\text{Na}(1.0)\text{M41}$, which possibly because the formation of high P-to-Ni ratio of Ni_5P_4 phase (Fig. 2, XRD analysis). The surface Na-to-P ratio of $\text{Ni}_2\text{P}/\text{Na}(x)\text{M41}$ decreased with increasing the Na mass fraction. This is understandable since the surface P decreases with Na mass fraction increase.

TEM

TEM images of the Ni₂P/M41, Ni₂P/Na(0.7)M41, and Ni₂P/Na(1.0)M41 catalysts are shown in Fig. 5. It can be seen from Fig. 5a that the average Ni₂P particle size of the Ni₂P/M41 catalyst is approximately 35 nm. Unlike the typical stacked morphologies of Mo and W sulfides, Ni₂P is not layered and forms spherical particles that can be well dispersed on supports [28]. The average Ni₂P particle sizes of Ni₂P/Na(0.7)M41 and Ni₂P/Na(1.0)M41 were 25.0 nm and 26.0 nm, respectively, which are smaller than that of Ni₂P/M41. And the average Ni₂P particle sizes correspond with the results of XRD analysis (See *D_c* in Table 1). The Ni₂P particle sizes of Ni₂P/Na(0.7)M41 (Fig. 5b) and Ni₂P/Na(1.0)M41 (Fig. 5c) were more uniform and an improved Ni₂P dispersion can be seen in comparison with Ni₂P/M41. With increasing the Na mass fraction from 0.7 to 1.0, the particle sizes changed little. Combined with XRD analysis, the increase of the Ni₂P peak intensities with increasing the Na mass fraction, one can conclude that addition of Na promotes formation of more Ni₂P particles on the surface.

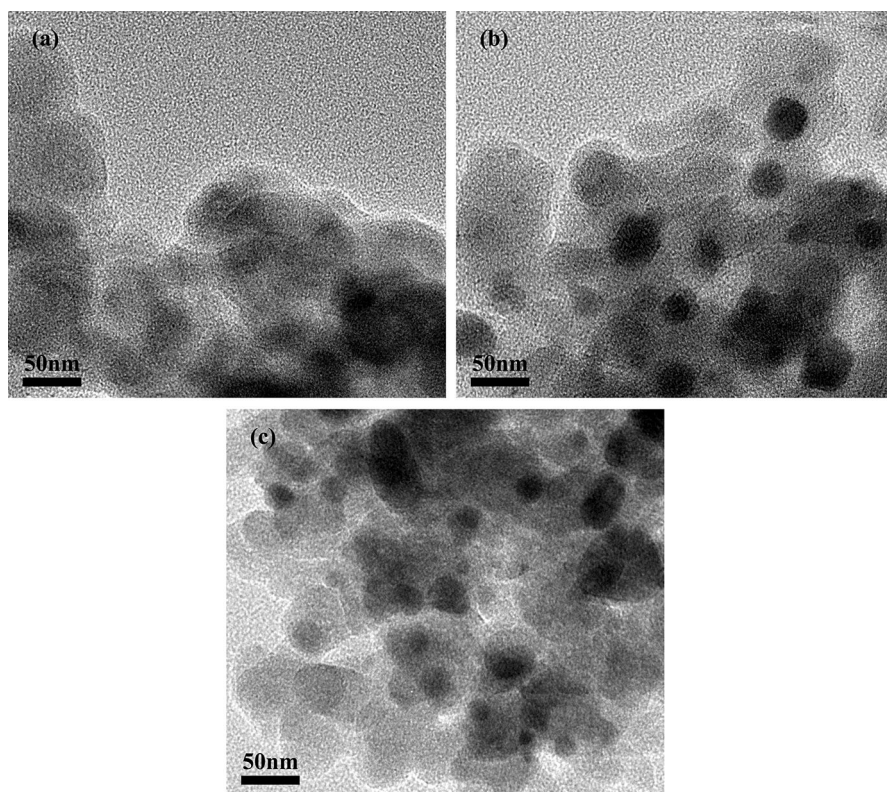


Fig. 5 TEM spectra of **a** Ni₂P/M41, **b** Ni₂P/Na(0.7)M41, and **c** Ni₂P/Na(1.0)M41

HDS activity

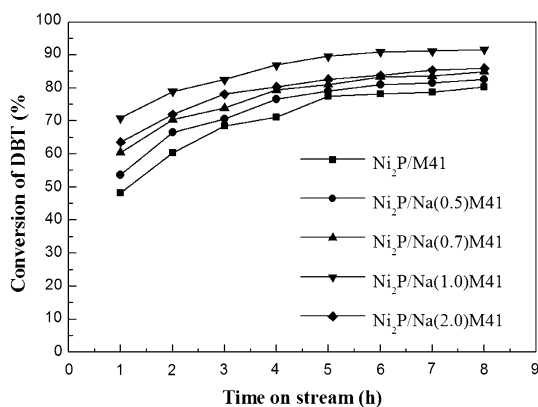
According to the literature [29], there are two parallel reaction pathways in the DBT HDS reaction, which are direct desulfurization (DDS) and hydrogenation (HYD). DDS is responsible for the formation of biphenyl (BP) and a small amount of the formed BP further transforms into cyclohexylbenzene (CHB), while HYD is mainly responsible for the formation of CHB. Because the transformation of BP into CHB is negligible in the HDS reaction, the selectivity of DDS is almost equal to the BP selectivity, and HYD selectivity is equal to that of the CHB selectivity.

The $\text{Ni}_2\text{P}/\text{M41}$ and $\text{Ni}_2\text{P}/\text{Na}(x)\text{M41}$ catalysts are evaluated by the HDS of DBT, and the results are shown in Fig. 6. As can be seen from Fig. 6, the DBT conversions for all samples increased with time on stream initially, during which more active intermediate phase gradually formed, and then tended to stabilize, showing the intermediate phase was completely formed. The active intermediate phase is regarded as a superficial phosphosulfide with a stoichiometry represented by NiP_xS_y , which is more active than Ni_2P phase [21]. The DBT conversion of $\text{Ni}_2\text{P}/\text{M41}$ reached the value of about 80.3% after 8 h. It is noted that the DBT conversion of $\text{Ni}_2\text{P}/\text{Na}(x)\text{M41}$ initially increased and then decreased with increasing the Na mass fraction. The $\text{Ni}_2\text{P}/\text{Na}(1.0)\text{M41}$ catalyst showed the maximum HDS activity of 91.6% after 8 h, which was 14.0% higher than that of $\text{Ni}_2\text{P}/\text{M41}$ without Na. This result is contrary to the trend of the P-to-Ni ratio of $\text{Ni}_2\text{P}/\text{Na}(x)\text{M41}$ (Table 2), which has a maximum value at $x = 1.0$. The enhanced HDS activity may be attributed to the smaller size (TEM) and better dispersion of the active Ni_2P phase (CO uptake), as well as the lower coverage of phosphorus on their surfaces (XPS analysis).

Temperature, 613 K; pressure, 3.0 MPa; H_2 -to-oil ratio, 550 (V/V); WHSV, 2.5 h^{-1} .

The DBT conversions obtained at $T = 553 \text{ K}$, $p = 3.0 \text{ MPa}$, $\text{WHSV} = 2.5 \text{ h}^{-1}$, and H_2 -to-oil ratio = 550 (V/V), and CO uptake were used to calculate the HDS TOF for the samples and the results are presented in Table 1. As can be seen from Table 1, the HDS TOF of $\text{Ni}_2\text{P}/\text{M41}$ is low ($3.2 \times 10^{-3} \text{ s}^{-1}$). The TOF of the $\text{Ni}_2\text{P}/\text{Na}(x)\text{M41}$ significantly increased, reaches maximum at $x = 1.0$ (the TOF was

Fig. 6 The conversion of DBT over the $\text{Ni}_2\text{P}/\text{Na}(x)\text{M41}$ catalysts

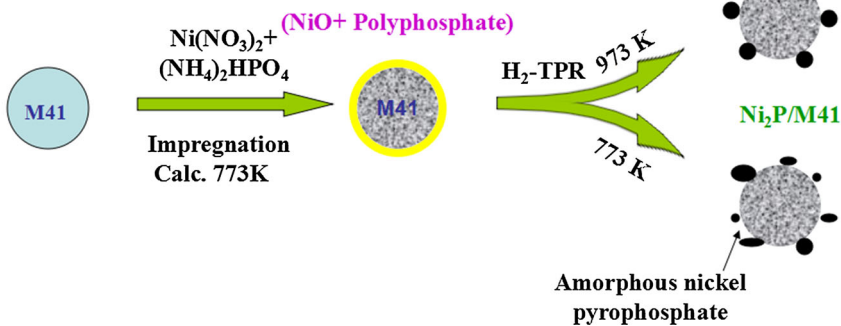


$3.6 \times 10^{-3} \text{ s}^{-1}$), and then decreased upon increasing the Na mass fraction. This indicates that more active Ni₂P phase was generated by addition of Na.

The effect of Na element on the HDS catalytic selectivity was also investigated in our study. Table 1 shows the selectivities of DBT over Ni₂P/M41 and Ni₂P/Na(x)M41 to BP and CHB. For all the samples, BP is formed in greater proportions, indicating that DBT primarily removed by the DDS pathway over all the catalysts [30]. Moreover, the BP selectivity of Ni₂P/M41 was 85.2%, and the BP selectivity of Ni₂P/Na(x)M41 catalyst decreased slightly with increasing the Na mass fraction. This result indicates that addition of Na has not dramatically changed for the HDS route [31].

Synthetic mechanism

It is well known that the reduction of metal nickel salt together with ammonium phosphate requires high temperature (973–1273 K) even with hydrogen [32]. Sawada et al. [15] studied the effect of Na addition on rhodium phosphide (Rh₂P) formation over MFI zeolite, SiO₂, and Al₂O₃; they found that the (NH₄)₂HPO₄ transforms into a polyphosphate such as diphosphate, tripolyphosphate, and tetrapolyphosphate over the MFI zeolite, and SiO₂ during the calcination process. The formation of AlPO₄ upon calcination is inevitable, but Na addition could weaken the interaction between the phosphate and Al. The reduction of polyphosphate is more difficult in comparison with the phosphate and the Na addition inhibits formation of polyphosphates [16]. This indicates that the amount of polymerized P–O–P bonds, which have stronger bonding than P–O–H in the precursor of phosphide catalyst, is decreased by Na addition [15]. The Na preferentially interacts with phosphate to suppress formation of stronger P–O–P bonds, which produced the phosphide catalyst at a lower reduction temperature. Both of the TPR profiles and XRD measurement showed that reducibility of phosphates in the Rh-P catalyst was remarkably enhanced by the addition of Na in the MFI support [15]. They explain the decrease in reduction temperature by addition of Na as Na interacts with phosphate to form sodium phosphate, such as NaH₂PO₄, in the impregnation step of catalyst preparation. Therefore, Na addition inhibits the formation of polyphosphate and decreases the reduction temperature. On the basis of the above discussion, a possible synthetic mechanism of the Ni₂P/M41 and Ni₂P/Na-M41 catalysts may be proposed to explain the effect of Na addition on the reduction temperature (Scheme 1). After calcination, Na species on Na-M41 existed in the form of Na which interacted with M41 and some NaNO₃. Therefore, the Na preferentially interacts with phosphate to generate the sodium phosphate during the impregnation step, and the formation of polyphosphate is inhibited. Hence, the addition of Na into the catalyst dramatically decreases the reduction temperature of Ni₂P/Na-M41 catalyst. For the Ni₂P/Na-M41 catalyst, the Ni₂P phase was generated at the reduction temperature of 773 K, which is at least 200 K lower than the reduction temperature of conventional phosphate (973–1273 K). However, without adding Na, the (NH₄)₂HPO₄ transforms into polyphosphate during the calcination process and the resistance of polyphosphate reduction becomes larger. The strong P–O–P

Ni₂P/Na-M41:**Ni₂P/M41:**

Scheme 1 Proposed synthetic mechanism of the Ni₂P/Na-M41 catalysts

bands are difficult to reduce at 773 K; therefore, the amorphous nickel pyrophosphate was obtained at this temperature (XRD analysis).

Conclusions

In this paper, Ni₂P/Na(x)M41 catalysts with different Na mass fractions and a higher HDS property have been successfully prepared at a lower reduction temperature (773 K), and the effect of Na mass fraction in the Ni₂P/Na(x)M41 on the HDS activities was investigated. Both XRD analysis and TEM photos indicate the incorporation of Na is beneficial for dispersion of Ni₂P particles. During the calcination process, the phosphate transforms into a polyphosphate such as diphosphate, tripolyphosphate, and tetrapolyphosphate. Therefore, a high reduction temperature is indispensable, mainly due to the polymerized P–O–P bonds in the precursor of phosphide catalyst. The addition of Na into the catalyst can dramatically decrease the reduction temperature of the catalyst (about 200 K). This is possibly because the Na preferentially interacts with phosphate to generate the sodium phosphate and, therefore, suppresses the formation of stronger P–O–P bonds. As a result, the amount of polymerized P–O–P bonds in the precursor of phosphide catalyst, which have stronger bonding than P–O–H, is decreased by Na addition. In addition, the incorporation of Na suppresses the enrichment of P on the surface of the catalyst and leads to more exposed Ni sites, which also improves the

CO uptake. By this means, the reduction temperature of Ni₂P/Na(*x*)-MCM-41 catalyst was 773 K, which is decreased by about 200 K as compared to that of the conventional phosphate (973–1273 K). The Ni₂P/Na(*x*)-MCM-41 catalyst with *x* = 1.0 showed the maximum DBT HDS activity of 91.6%, which was 14.0% higher than that of Ni₂P/M41-773 without Na (80.3%).

Acknowledgements The authors acknowledge the financial supports from the National Natural Science Foundation of China (21276048).

References

1. M. Egorova, R. Prins, *J. Catal.* **255**, 417 (2004)
2. Q.Y. Li, P.Y. Wu, L. Lan, H. Liu, S.F. Ji, *Catal. Today* **216**, 38 (2013)
3. H.Y. Zhao, S.T. Oyama, H.J. Freund, R. Włodarczyk, M. Sierka, *Appl. Catal. B* **164**, 204 (2015)
4. X. Li, Z.C. Sun, A.J. Wang, X.N. Yang, Y. Wang, *Appl. Catal. A* **417**, 19 (2012)
5. S. Tian, X. Li, A. Wang, R. Prins et al., *Angew. Chem. Int. Edit.* **55**, 4030 (2016)
6. C.P. Jiménez-Gómez, J.A. Cecilia, R. Moreno-Tost et al., *ChemCatChem* **9**, 2881 (2017)
7. H. Song, F.Y. Zhang, H.L. Song, X.W. Xu, F. Li, *Catal. Commun.* **69**, 59 (2015)
8. Y.Y. Shu, S.T. Oyama, *Carbon* **43**, 1517 (2005)
9. H. Loboué, C. Guillot-Deudon, A.F. Popa, A. Lafond, B. Rebours, C. Pichon, T. Cseri, G. Berhault, C. Geantet, *Catal. Today* **130**, 63 (2008)
10. K.S. Cho, H.R. Seo, Y.K. Lee, *Catal. Commun.* **12**, 470 (2011)
11. H. Song, M. Dai, H.L. Song, X. Wan, X.W. Xu, Z.S. Jin, *J. Mol. Catal. A- Chem.* **385**, 149 (2014)
12. H. Song, M. Dai, H.L. Song, X. Wan, X.W. Xu, C.Y. Zhang, H.Y. Wang, *Catal. Commun.* **43**, 151 (2014)
13. H. Song, M. Dai, H.L. Song, X.X.W. Xu, *Appl. Catal. A* **462–463**, 247 (2013)
14. A.I. d'Aquino, S.J. Danforth, T.R. Clinkingbeard, B. Ilic, L. Pullan, M.A. Reynolds, B.D. Murray, M.E. Bussell, *J. Catal.* **335**, 204 (2016)
15. A. Sawada, Y. Kanda, M. Sugioka, M. Uemichi, *Catal. Commun.* **56**, 60 (2014)
16. H.I. Meléndez-Ortiz, L.A. García-Cerda, Y. Olivares-Maldonado, G. Castruita, J.A. Mercado-Silva, Y.A. Perera-Mercado, *Ceram. Int.* **38**, 6353 (2012)
17. V. Teixeira da Silva, L.A. Sousa, R.M. Amorimb, L. Andrini, S.J.A. Figueroa, F.G. Requejo, F.C. Vicentini, *J. Catal.* **279**, 88 (2011)
18. Z.Y. Pan, R.J. Wang, Z.Y. Nie, J.X. Chen, *J. Energy Chem.* **25**, 418 (2016)
19. X. Wang, P. Clark, S.T. Oyama, *J. Catal.* **208**, 321 (2002)
20. S.T. Oyama, X. Wang, Y.K. Lee, W.J. Chun, *J. Catal.* **221**, 263 (2004)
21. S.T. Oyama, X. Wang, Y.K. Lee, K. Bando, F.G. Requejo, *J. Catal.* **210**, 207 (2002)
22. K.A. Layman, M.E. Bussell, *J. Phys. Chem. B* **108**, 10930 (2004)
23. I.K. Tamás, V. Zdeněk, G.P. Dilip, R. Ryong, S.K. Hei, J.M.H. Emiel, *J. Catal.* **253**, 119 (2008)
24. J.N. Kuhn, N. Lakshminarayanan, U.S. Ozkan, *J. Mol. Catal. A* **282**, 9 (2008)
25. L. Song, S. Zhang, Q. Wei, *Catal. Commun.* **12**, 1157 (2011)
26. H. Song, M. Dai, Y.T. Guo, Y.J. Zhang, *Fuel Proces. Technol.* **96**, 228 (2012)
27. P. Liu, J.A. Rodriguez, *J. Am. Chem. Soc.* **127**, 14871 (2005)
28. H. Song, J. Wang, Z.D. Wang, H.L. Song, F. Li, Z.S. Jin, *J. Catal.* **311**, 257 (2014)
29. S.T. Oyama, T. Gott, K. Asakura, S. Takakusagie, K. Miyazakib, Y. Koiked, K.K. Bando, *J. Catal.* **268**, 209 (2009)
30. H. Song, X.W. Xu, M. Dai, H.L. Song, *Chem. J. Chin. Univ.* **34**, 2609 (2013)
31. S.T. Oyama, Y.K. Lee, *J. Catal.* **258**, 393 (2008)
32. R. Prins, M.E. Bussell, *Catal. Lett.* **142**, 1413 (2012)